Algal Research 74 (2023) 103172

Contents lists available at ScienceDirect

Algal Research

journal homepage: www.elsevier.com/locate/algal

Light-dependent metabolic shifts in the model diatom *Thalassiosira pseudonana*

Nerissa L. Fisher [a], Kimberly H. Halsey [b], David J. Suggett [a,1], Michelle Pombrol [b], Peter J. Ralph [a], Adrian Lutz [c,2], E. Maggie Sogin [d,3], Jean-Baptiste Raina [a], Jennifer L. Matthews [a,*]

[a] Climate Change Cluster, University of Technology Sydney, Ultimo 2007, NSW, Australia
[b] Department of Microbiology, Oregon State University, Corvallis, OR, USA
[c] Metabolomics Australia, University of Melbourne, Parkville 3052, VIC, Australia
[d] Max Planck Institute for Marine Microbiology, Bremen, Germany

ARTICLE INFO

Keywords:
Metabolomics
Transcriptomics
Diatom
Thalassiosira
Light intensity
Phytoplankton

ABSTRACT

Diatoms are major producers of carbon and energy in aquatic ecosystems, however their ability to rapidly and successfully acclimate to wide ranging irradiances is poorly understood at the biochemical level. We applied complementary transcriptomic and metabolomic approaches using the model centric diatom *Thalassiosira pseudonana* to understand mechanisms regulating cell acclimation and growth under high and low light intensities. The integration of these omics data revealed specific mechanisms that shifted carbon and energy fluxes in *T. pseudonana* depending on light-driven growth rate. To support a growth rate of >1 d^{-1} in high light, cells upregulated metabolic pathways involved in the production of long chain fatty acids, glycolic acid, and carbohydrates. Under low light, cells maintained a growth rate of ≤0.2 d^{-1} by conserving photosynthetic energy through upregulation of carbon retention pathways (e.g., gluconeogenesis, glyoxylate cycle). The few significant metabolites detected in low light acclimated cells were associated with light harvesting, energy storage, and signalling. In particular, our metabolite data revealed that eicosanoic acid, a metabolite commonly involved in cellular signalling, may poise light limited cells for fast metabolic remodelling with improving light conditions. The combined physiological, gene expression and metabolite profiling data revealed key metabolic switch points that underpin diatom success and could be leveraged in cell-based models for predictions and manipulations of cell growth or bio-production.

1. Introduction

Diatoms are one of the most diverse and productive phytoplankton groups in aquatic systems, driving more net production than tropical rainforests or savannahs [1–4]. In the marine environment, diatoms thrive and bloom under physically complex conditions, particularly in coastal waters where nutrients are typically not limiting growth, and light is highly dynamic [5–7]. A wealth of research has helped explain how these various environmental factors regulate bloom formation [8], including diatom photo-physiological responses to nutrient limitation [9–12] and light stress [13,14] as well as corresponding energy allocation strategies that are activated to sustain optimal fitness [15–20].

Abbreviations: AMDIS, Automated Mass spectral Deconvolution and Identification System; AOX, alternative oxidase; BCAA, branched-chain amino acid; CBB, Calvin-Benson-Bassham; FDR, false detection rate; FRRf, Fast Repetition Rate fluorometer; GDC, glycine decarboxylase p-protein; KEGG, Kyoto Encyclopedia of Gene and Genomes; OAA, oxaloacetate; PCA, principal component analysis; PEP, phosphoenolpyruvate; PFD, photon flux density; PLS-DA, partial least squares discriminant analysis; POC, particulate organic carbon; PON, particulate organic nitrogen; SAM, significant analysis of metabolites; SCF, spectral correction factor; SHMT, serine hydroxymethyltransferase; TCA cycle, tricarboxylic acid cycle; VANTED, Visualization and Analysis of Networks containing Experimental Data.

* Corresponding author.
E-mail address: Jennifer.matthews@uts.edu.au (J.L. Matthews).
[1] Present address: King Abdullah University of Science & Technology (KAUST), Thuwal 23955, Saudi Arabia.
[2] Present address: Department of Microbiology & Immunology, the University of Melbourne, Parkville 3052, VIC, Australia.
[3] Present address: University of California, Merced, 5200 North Lake Rd, Merced, CA, USA.

https://doi.org/10.1016/j.algal.2023.103172
Received 16 January 2023; Received in revised form 28 May 2023; Accepted 7 June 2023
Available online 13 June 2023

Rapid and high-throughput approaches that can capture photophysiological properties (e.g., bio-optics and active fluorometry [21–26]) have been useful to gain an understanding of how diatoms respond to dynamic environmental conditions. Photophysiology under different light regimes, particularly for the model diatom *Thalassiosira pseudonana*, has been largely examined through fluorescence-based assays of photosystem II (PSII) operation (e.g., [27–30]) and bulk cellular constituents (e.g., C and N allocation [31–34]). "Omics" platforms, such as metabolomics, complement current knowledge of diatom photophysiology by characterizing chemical fingerprints that arise in response to changing environments, making it possible to resolve the metabolic processes at play. Connecting "omics" platforms (e.g., genomics, transcriptomics and proteomics) in diatoms helps to understand the molecular bases of physiological responses [12,35–37] and can elucidate the underlying function of targeted metabolites [38–40]. However, the metabolic responses and the molecular pathways underpinning physiological responses, and so enable diatoms to thrive in widely varying light conditions, remains a black box.

Transcriptomics have uncovered the regulatory networks responsible for fine-tuning diatom biology to changing environments (e.g., [41–45]). However, the fundamental nature by which phytoplankton appear to respond to rapid environmental changes is via post-translational modification of protein [46,47] and metabolite pools [48–50]. While gene expression levels alone cannot predict phenotypes, metabolites are direct products of enzymatic reactions and thus provide a functional readout of the cellular networked response to an environment [51]. The model diatom *T. pseudonana* has been widely used in many omics-based studies [52], however studies exploring metabolomic responses in diatoms have been limited to community interactions [53,54], the exometabolome [55,56], nutrient stress [57–59], and salinity and pH (CO_2 concentration, [48]). Together, these studies have improved our understanding of the dynamic cellular processes of *T. pseudonana* but have largely overlooked the effect of light. Consequently, we still do not know whether photophysiological changes match dynamic reorganization of cellular metabolism under light-driven growth (e.g., [60]).

Here, we used transcriptomics and metabolomics to study how metabolic networks of *T. pseudonana* are altered under controlled manipulations of light-driven balanced growth. We hypothesize that transcriptomics and metabolomics profiles of *T. pseudonana* will be markedly different under high versus low light-driven growth and will expose the cellular networks underpinning light-driven growth. We initially examined *T. pseudonana* gene expression when acclimated to growth under different constant light intensities, which pinpointed several metabolic pathways that were differentially regulated between treatments. Based on these transcriptomic indicators, we subsequently conducted a follow-on experiment to examine the corresponding metabolite profiles under light acclimated growth. Together, these data provide a platform for conceptual integration (sensu [61]) of the genetic and chemical responses to light regime. Our work revealed fundamental shifts in central metabolism used to direct carbon and energy toward biosynthesis for rapid cell growth or into pathways that conserve photosynthetic energy to facilitate slow steady growth. These key metabolic switch points may be leveraged in future cell-based models for predictions and manipulations of cell growth or bio-production.

2. Materials and methods

2.1. Gene expression study

2.1.1. Culture conditions and maintenance

The experimental design used in this study is identical to the one previously described in Fisher and Halsey [19]. Briefly, *T. pseudonana* (CCMP1335) was grown in f/2 + Si medium [62] supplemented with 0.17 μM Na_2SeO_3, and 250 and 50 μM nitrate and phosphate, respectively [63], to avoid nutrient limitation. Cultures were grown at 18 °C in continuous cultures that were optically thin [64] at 200 and 5 μmol photons m^{-2} s^{-1} for a high or low light treatment, respectively, under constant light [24:0 light:dark (L:D) cycle]. All cultures were acclimated to their growth irradiances for at least 10 generations and verified to be in balanced growth when cell concentration varied by <5 % over 3 days before harvest. Data were collected from three independent continuous cultures for low light treatment (due to slow culture growth) and five independent continuous cultures for the high light treatment as per [19]. Samples of 300 mL at a density of about 1.5×10^6 cells mL^{-1} were collected onto 0.2 μm nucleopore filters, flash-frozen in liquid nitrogen, and stored at −80 °C until RNA extraction and analysis.

The culturing methods used in all experiments ensured that cells were maintained in exponential growth phase by removing a known volume of culture and replacing it with fresh media according to

$$\mu = \frac{D}{V}$$

where μ is the population growth rate (d^{-1}), D is the dilution rate (mL d^{-1}) and V is the volume of the culture (mL). The difference between continuous (used in the transcriptomics work) and semi-continuous (used in the metabolomics work, see below) culturing is the frequency of dilution, whereby dilution of cultures grown for transcriptomics occurred continuously using a digital peristaltic pump (Minipuls Gilson; Middleton, WI USA) and cultures grown for metabolomics were diluted once or twice daily manually.

2.1.2. Total RNA extraction and sequencing

Following established procedures [46], total RNA was extracted from filters using a Qiagen RNeasy Mini Kit with the addition of silica beads (0.5 mm) to the lysis buffer. Filters, beads, and lysis buffer were vortexed together; supernatant was then filtered through Qiashredder columns to remove large particles. Eluted RNA was treated off-column with RNase-free DNase according to manufacturer's recommendations. mRNA isolation and library preparation were performed using the PrepX PolyA mRNA Isolation Kit and RNA-Seq for Illumina Library Kit from Takara Bio USA, Inc. These steps were carried out on an Apollo 324 robotic system by the Center for Genome Research and Computing at Oregon State University. RNA-derived reads were sequenced as a 150 bp single-end library via Illumina HiSeq 3000.

2.1.3. RNA-Seq quality trimming and sequence alignment

FastQC [65] was used to check GC content and per-base quality scores in each sample. Raw reads were quality trimmed and filtered using Sickle v1.33 [66] with the options "-q 33 -l 50". The first option sets the quality score threshold for trimming to 33, while the second option discards all reads that are shorter than 50 base pairs after trimming. Sequencing adapters were not removed, as previous studies have shown that adapters do not significantly affect alignments to reference genomes and aggressive trimming can lead to bias and poorer results [67,68]. The *T. pseudonana* reference genome was obtained from NCBI in GFF format (accession number GCA_000149405.2) and converted to GTF using gffread. Reads were aligned to the reference genome using HISAT2 v2.1.0 [69] with the option "–dta". HISAT2 is a splice-aware aligner that generates alignments more quickly and using less memory than older alignment software such as BowTie or BWA [70]. The "–dta" option tells the program to report alignments in a format that is tailored to transcriptome assemblers like StringTie. HISAT2 created sequence alignment/map files for each sample. These files contain the alignments in the order that the sequences occurred in the input FASTQ files. SAMtools v1.3 [71] was used to sort the alignments with respect to their genomic positions and then converted the files to binary alignment/map files, which facilitates more rapid computation. Coverage depth of the genome was calculated using the "genomeCoverageBed" command with the "-ibam" option in BEDTools v2.25.0 [72]. StringTie v1.3.3 [73] was used to assemble putative transcripts and generate counts tables for use

in DESeq2. First, putative transcripts were assembled using the reference annotation file downloaded from NCBI. Then, data from all samples were merged into a single file using the command "stringtie –merge." Finally, "stringtie -eB" was used to calculate transcript abundances and generate counts tables structured for Ballgown (DESeq2 also accepts these counts tables as input). DESeq2 v1.20.0 [74] was used to perform differential expression analysis and create exploratory visualizations.

2.1.4. Quality control and differential expression analysis

Prior to differential expression analysis, we transformed the count data to make it homoscedastic. We used the regularized log (rlog) transformation (log2 scale normalized with respect to library size) for downstream exploratory analyses and visualizations. DESeq2 [75] tests for differential expression by 1) normalizing sequencing depth between samples using an estimate of "size factors", 2) estimating dispersion across all samples, and 3) fitting a negative binomial generalized linear model. DESeq2 uses a Wald test to calculate a *p*-value for differential expression; these *p*-values are then adjusted for multiple testing using the Benjamini-Hochberg correction. DESeq2 also assigns log2 fold change values for each gene. Under the default parameters in DESeq2, the null hypothesis is that a gene is *not* differentially expressed between treatments. The alternative hypothesis is that a gene *is* differentially expressed between treatments. These default parameters were used to test for differential expression of genes between the high light and low light treatment groups. However, it cannot be assumed that genes with Benjamini-Hochberg adjusted *p*-values larger than our significance threshold are stably expressed. The parameters "altHypothesis = lessAbs" and "lfcThreshold = *x*" were added to the results function to test for stable expression. The parameter *x* defines the threshold for log2 fold change. Setting a log2 fold change threshold to 1 (fold change = 2) yielded 4270 significant genes.

The Bioconductor package KEGGREST [76] was used to access gene annotations from the KEGG database; functional annotation was limited to KEGG pathways. Pathview Web [77] was used to visualize relative expression of genes within KEGG pathways. Following quality trimming, sequence alignment, quality control measures and functional annotation, the results were compared between light treatments using fold change cut-off of 2 with an adjusted *p*–value of 0.05.

2.2. Metabolite profiling study

2.2.1. Culture conditions and maintenance

Following the experimental design used for the transcriptomics study, *T. pseudonana* (CCMP1335) was grown in a Multi-Cultivator (MC 1000-OD, Photon Systems Instrument (PSI), Drasov, Czech Republic), whereby light intensity and dose was altered across two different experimental treatments by modifying the light delivered by the PSI Multi-Cultivator LEDs (cool white light). Growth light intensity was set to 200, 60 or 5 µmol photons m^{-2} s^{-1} for a high, medium or low light treatment, respectively, but was delivered by a different light source (spectral quality) than for the parallel transcriptomics study. Therefore, a spectral correction factor (SCF) of 0.71 was used to weight the white LED light source (Multi-Cultivator) to the cool-white fluorescent tube used in the transcriptomics study as per Hughes et al. [11] using fluorescence excitation spectra (400–700 nm) previously collected for *T. pseudonana* [78]. Consequently, the spectrally equivalent light intensity experienced by *T. pseudonana* under the white LED light source was 143, 43 and 3.6 µmol photons m^{-2} s^{-1} for these light treatments, and importantly, the magnitude of the growth intensity differences between the high and low light treatments used for the transcriptomics and metabolomics studies were the same.

T. pseudonana cultures were grown in the same f/2 + Si medium described above and subjected to two different experiments. First, cultures were grown in parallel under constant light (24:0 L:D) set at 200, 60 or 5 µmol photons m^{-2} s^{-1}, referred to as HC, MC and LC, respectively. In the second experiment, cultures were grown under pulsed light (12:12 L:D) at 200 and 5 µmol photons m^{-2} s^{-1}, referred to as HP and LP, respectively. Four independent biological replicates were grown for each light treatment. All cultures were optically thin and maintained for at least seven generations using semi-continuous culturing technique to ensure balanced growth [64], which was confirmed using fluorometry (see below). Cultures were maintained at 20 °C, which was 2 °C higher than used in the transcriptomic study, but variation between 18 and 20 °C gave comparable physiological responses in *T. pseudonana* [79].

2.2.2. Photophysiology measurements

Small aliquots (3–4 mL) were drawn daily from each culture vessel under each light treatment for cell counts and photophysiology. Daily cell samples were preserved using glutaraldehyde (Sigma-Aldrich) until counted by chlorophyll fluorescence for 60 s at a rate of 30 µL min^{-1} via flow cytometry (CytoFlex S, Beckman Coulter, Miami, FL USA). Daily photophysiological assessment for each light treatment was performed on samples that were first low light (<10 µmol photons m^{-2} s^{-1}) acclimated for 5 min (modified as per Suggett et al. [80]) to ensure full oxidation of the photosynthetic electron transport chain and relaxed nonphotochemical quenching processes before measuring fluorescence using a *FastOcean* Fast Repetition Rate fluorometer (FRRf; S/N: 12-8679-007) coupled to a bench-top FastAct unit (Chelsea Technologies Group Ltd., UK). The FRRf was programmed to deliver single turnover inductions consisting of 100 flashlets of 1.1 µs at 2.8 µs intervals to retrieve values of the maximum photochemical efficiency (F_v/F_m, dimensionless) using the biophysical model of Kolber et al. [81]. A culture was considered to be in balanced growth for sampling when values of F_v/F_m were consistent (<5 % variance) across 3 consecutive days. Acclimation occurred over 2–5 weeks, depending on growth rate.

2.2.3. Chlorophyll and particulate organic carbon/nitrogen

Samples for chlorophyll were taken as 5 mL aliquots in duplicate from each biological replicate, each filtered onto a GF/F (Whatman, 25 mm) and extracted overnight at −20 °C in 90 % acetone. Absorption was measured using a spectrophotometer (Aligent Technologies, Cary 60 UV–Vis) set at wavelengths 630, 657, 664, and 750 nm to calculate chlorophyll *a* concentration according to Ritchie [82]. Cellular particulate organic carbon (POC) and nitrogen (PON) were also measured in duplicate for each biological replicate, filtering 3–5 mL aliquots onto pre-combusted GF/F filters (Whatman, 25 mm). Culture filtrate (5 mL) was also collected as background subtraction. Filters were stored at -20 °C until analysis on an elemental analyzer (LECO, Baulkham Hill, Australia).

2.2.4. Metabolomics sampling

Sampling was performed between 6 and 8 h following the onset of light for the pulse treatment to standardize for time of day. Samples were gently filtered under their respective growth irradiance prior to immediate flash freezing. This approach maintained light acclimated cells and best captured the metabolic profile under a particular light regime (as opposed to widely used protocols where cultures are pelleted using centrifugation in the dark). For each sample, a volume of culture (for specific volumes and cell concentrations per sample, see Table S1), was gently filtered to 1 mL using a 2 µm polycarbonate membrane filter and a 47 mm GF/F backing filter. Cells were maintained in suspension during filtration for ≤30 s by gently pipetting manually. The concentrated 1 mL culture was transferred to a 2 mL cryovial tube, immediately flash frozen in liquid nitrogen, and stored at −80 °C until extraction.

2.2.5. Metabolite extraction

Metabolite extraction followed in-house protocols adapted for marine algae [83]. Briefly, each 1 mL concentrated sample was lyophilized overnight at −82 °C under 0.1 mbar (Alpha 2-4 LDPlus, John Morris Scientific). To each dried sample, 450 µL 100 % methanol was added to extract the semi-polar metabolites and vortexed. Cell slurry was transferred to a clean 2 mL Eppendorf tube and an additional 450 µL 100 %

methanol was used to rinse the original tube and combined with cell slurry. Samples were (1) vortexed, (2) sonicated (FX10 Ultrasonic Cleaner, Unisonics Pty Ltd., Australia) for 20 min at 4 °C to rupture the cells, (3) incubated at room temperature on a rotating platform at 1000 rpm for 30 min and finally (4) centrifuged for 10 min at 13000 ×*g* at 4 °C to pellet cell debris. Supernatant was transferred and pellet re-suspended in 900 μL 50 % MeOH to extract the polar metabolites. The re-suspended pellet mixture followed steps 1–4 outlined above. Again, the supernatant was transferred and added to the supernatant collected earlier. The combined supernatant was vortexed and centrifuged to avoid collecting cell debris. An aliquot of 850 μL supernatant was added to 2 pre-weighed Eppendorf tubes (pre-dried in a SpeedVac (Eppendorf Concentrator 5301, Hamburg, Germany) overnight to remove moisture), then dried in a SpeedVac overnight at 30 °C and re-weighed to determine the methanol extractable diatom metabolite weight (i.e., 'metabolite extract weight'). To prepare samples for GC–MS, individual extracts were derivatized following Sogin et al. [84], a protocol designed to measure metabolites from samples containing high concentrations of salts. All derivatized samples were processed within one day after derivatization to avoid sample degradation and crystallization of MeOx.

2.2.6. Metabolite analysis/GC–MS processing

Derivatized samples were analyzed using a GC (Agilent 7890B) coupled to a single quadrupole mass selective detector (Agilent 5944A) and an autosampler (Agilent 7693) as described in Sogin et al. [84]. The method was retention time locked using a standard mixture of fatty acid methyl esters (Sigma Aldrich). Spectral components in each sample were separated, detected and identified during deconvolution using AMDIS (http://chemdata.nist.gov/mass-spc/amdis/). Compound identification was based on an in-house library of MS spectra, with retention indices based on n-alkane and the standard mixes [84]. Derivative peak areas from the GC–MS signal outputs were used to estimate relative abundance of individual metabolites. Data were then normalized to final area of the internal standard cholestane and then to sample 'metabolite extract weight'.

2.2.7. Metabolite data normalization

We normalized our data by 'metabolite extract weight' [83] instead of per cell or by the more traditional normalization metric, dry cellular biomass, due to unforeseen circumstances using the sampling protocol of concentrating culture volume down to a 1 mL sample (see 'Metabolomics sampling' section above). Upon freeze drying, this 1 mL concentrated sample was subject to salt contamination, which ruled out the option to normalize by cell material dry weight. In addition, normalization per cell was not ideal since the cell density of LP was found to be significantly lower than all other light treatment samples ($p < 0.05$, see Table S2 for independent *t*-test comparisons) and subject to both biological and methodological variation during the processing steps between cell density sample collection and metabolite extract [85]. Therefore, normalizing our data by 'metabolite extract weight' provided the most robust comparison across all light treatments.

2.2.8. Metabolite data processing/statistics

Physiological measurements were compared within and between light treatments using *t*-tests or ANOVAs (IBM SPSS Statistics v26) set to a false-detection corrected significance level of $p < 0.05$. Specifically, constant (HC, MC, LC) as well as pulse (HP, LP) light treatments were assessed using one-way ANOVAs followed by Tukey's multiple comparison test. Before using these parametric tests, we ensured that the data did not violate the assumptions of normality and homoscedasticity using Levene's and Shapiro-Wilk tests, respectively. If normality was violated, data were either square-root or log transformed and the distribution of residuals re-tested. If either assumption continued to be violated despite transformation, differences between constant light treatments were instead evaluated using a non-parametric ANOVA on ranks (i.e., Kruskal-Wallis test), followed by Dunnett T3 post-hoc test. Pulse (HP and LP) light treatments were statistically assessed using Student's *t*-test. All statistical tests were set to a significance level of $p < 0.05$.

Statistical analyses of metabolomics data were processed using the software package MetaboAnalyst 4.0 [86]. All data processed in MetaboAnalyst were log-transformed with no additional scaling. Principal component analysis (PCA) was first used to provide an unsupervised visual comparison of the metabolite profiles between treatments. Where no clear separation between the treatments was visible, a supervised partial least squares discriminant analysis (PLS-DA) was performed and assessed from ten-fold cross-validation based on Q^2 and goodness-of-fit (R^2) evaluated with permutation testing by prediction accuracy during training using 1000 iterations. To identify metabolites significantly different between treatments, significance analysis of microarray (SAM) plots with a false discovery rate (FDR) <10 % were performed. SAM assigns a significance score to each metabolite based on relative changes to standard deviation between repeated measurements while FDR signifies the portion of metabolites found to be significant by chance. SAM was used to identify significant metabolites because this approach works well with high-dimensional data and groups with low and/or unequal samples sizes [87,88]. To identify how metabolites significantly differed between specific treatments, one-way ANOVAs followed by Tukey's multiple comparison tests were used (following checks for normality and homoscedasticity as above).

Assembling identified metabolites, especially those found to be significant, into metabolic pathways was completed using the software package VANTED (http://vanted.ipk-gatersleben.de, [89]) based on numerical identifiers from the Kyoto Encyclopedia of Gene and Genomes (KEGG) database [90].

2.2.9. Conceptual integration of metabolic and transcriptomic profiles from constant light treatments

Given the independent nature of the transcriptomic and metabolomic experiments, we did not statistically compare omics data sets but rather conceptually integrated [61] patterns of metabolomic outcomes relative to transcriptional changes. This repeated study design allowed for independent tests of the same hypothesis. Genes and metabolites that were identified as significant were analyzed in a pathway context using KEGG pathways, then the data was integrated into a conceptual diagram showing the cellular pathways influenced by light-limited growth.

3. Results

3.1. Physiological effects of light treatment

Physiological responses captured during the metabolomics experiment demonstrated that the growth rate of *T. pseudonana* increased significantly with light intensity for both constant and pulse light doses, from ca. 0.12–0.18 to 1.12–1.17 d^{-1} (Table 1). Light intensities ranged from 5 to 200 μmol photons m^{-2} s^{-1} and growth rates were comparable between light dose treatments for the same intensity (i.e., HC vs. HP and LC vs. LP) despite the integrated daily photon dose for constant light being double that of the pulse light.

For the constant light treatments, Chl *a* content per cell (Chl *a* $cell^{-1}$) decreased, while both C and N content per cell (C $cell^{-1}$; N $cell^{-1}$) increased, with increasing light intensity (Table 1). The trends for Chl *a* $cell^{-1}$ observed under pulse light were consistent with constant light, but C $cell^{-1}$ and N $cell^{-1}$ were higher under lower light (Table 1). Regardless of light treatment (constant or pulse), C:N was higher under low light. F_v/F_m showed that cells in all treatments were highly efficient at harvesting light energy at PSII. For statistical comparison of samples with matching average photon flux density (PFD) across constant and pulse light dose treatments (HC-HP, LC-LP), an additional 2-way ANOVA was conducted to examine the influence of light dose, light intensity and the interactive effect of light dose and light intensity (Table S3). All variables, except Chl *a* $cell^{-1}$, were significantly different

Table 1
Physiological characteristics of *Thalassiosira pseudonana* measured at the time of metabolomics sampling during balanced acclimated growth to five different light regimes: Constant (high, medium, low) and Pulse (high, low) at 20 °C. ANOVA or Kruskal-Wallis (KW) test results are presented using F- or H-values, respectively, for constant light treatments followed by Tukey's or Dunnett T3 post-hoc analysis, respectively, with differences between individual cell characteristics and light intensity designated by superscripted letters. For pulse light treatments, Student's *t* – test results are shown using *t*-values. For 2-way ANOVA test results for light treatments of equal average PFD (HC-HP, LC-LP) see Table S3.

Light dose (L:D cycle)	Light treatment	Avg PFD (μmol photons m^{-2} s^{-1})	Growth rate (d^{-1})	Cells mL^{-1} ($\times 10^6$)	Chl *a* $cell^{-1}$ (pg)	C $cell^{-1}$ (pg)	N $cell^{-1}$ (pg)	C:N	F_v/F_m
Constant (24:0)	High	**200**	**1.17**[a] (0.08)[$]	**2.35** (0.29)	**0.30**[a] (0.04)	**14.61**[a] (1.39)	**2.38**[a] (0.28)	**6.16**[a] (0.16)	**0.52**[a] (0.00)
	Med	**60**	**1.06**[a] (0.03)	**2.16** (0.11)	**0.28**[a] (0.01)	**10.23**[b] (0.45)	**1.75**[b] (0.12)	**6.00**[a] (0.62)	**0.53**[a] (0.00)
	Low	**5**	**0.18**[b] (0.00)	**1.59** (0.12)	**0.50**[b] (0.03)	**10.32**[c] (0.61)	**1.13**[c] (0.10)	**9.34**[b] (0.69)	**0.54**[b] (0.00)
	ANOVA or KW	F/H	H = 8.38	F = 3.92	F = 17.64	F = 74.06	F = 15.65	H = 9.10	F = 6.23
		p value[*]	**<0.05**	>0.05	**<0.05**	**<0.05**	**<0.05**	**<0.05**	**<0.05**
Pulse (12:12)	High	**200**	**1.12** (0.10)	**1.77** (0.15)	**0.15** (0.01)	**8.87** (0.96)	**1.27** (0.16)	**7.55** (0.30)	**0.55** (0.00)
	Low	**5**	**0.12** (0.01)	**0.80** (0.03)	**0.38** (0.03)	**17.70** (1.05)	**1.86** (0.18)	**9.80** (1.06)	**0.53** (0.00)
	Student's *t*-test	*t*-Value	3.52	7.18	6.92	15.30	8.81	14.07	166.29
		p value[*]	**<0.05**	**<0.05**	**<0.05**	**<0.05**	>0.05	**<0.05**	>0.05

[$] Values in parentheses represent SE of the mean for at least 3 independent biological replicates.
[*] Significant *p* values ($p < 0.05$) in bold.

for either light dose or light intensity and a significant interactive effect was evident for C $cell^{-1}$, N $cell^{-1}$ and F_v/F_m.

Detailed physiological data accompanying the HC and LC transcriptomics were previously reported by Fisher and Halsey [19], and a comparison of major physiological characteristics for both the transcriptomics and metabolomics HC and LC samples are shown in Table S4. While absolute values of all variables somewhat differed between parallel experiments, all reported data varied in the same direction when HC was compared to LC. Overall, both experiments elicited consistent emergent physiological outcomes for the two constant light treatments.

3.2. Light-dependent gene expression of T. pseudonana

A total of 2904 genes (25 % of the genome) were differentially expressed in HC compared to LC, using a fold change >2 cut-off (adjusted *p*-value < 0.05). Of these genes, 1410 were upregulated in LC compared to HC and 1494 were downregulated in LC compared to HC. While the vast majority of the differentially expressed genes were unannotated in the KEGG database, fatty acid metabolism, nucleotide sugar metabolism, and valine, leucine, and isoleucine degradation accounted for the most represented categories of genes upregulated in LC (Fig. 1; Table S5). Two of the most highly upregulated genes in LC were involved in carbon metabolism: *PDK1_2* encoding pyruvate-phosphate dikinase increased 6.7-fold and *PCK1* encoding a phospho-enolpyruvate carboxykinase increased 7.3-fold. Genes encoding enzymes in the glyoxylate cycle and transport into the peroxisome, where the glyoxylate cycle occurs, were also upregulated in LC. Genes encoding proteins associated with photorespiration (glycine decarboxylase and serine hydroxymethyltransferase) and the TCA cycle (malate dehydrogenase, isocitrate dehydrogenase, fumarate hydratase) were upregulated in HC (Fig. 2). Although some of these genes fell below the fold change >2 cut-off, they were significantly differentially expressed between treatments ($p < 0.05$) (Table S5).

3.3. Light-dependent effects on metabolic profiles

Distinctions in metabolite profiles were evident between light intensity (i.e., high, medium and low) and light dose (i.e., constant or pulse) treatments via spatial separation in the PCA (Fig. 3A & B) and

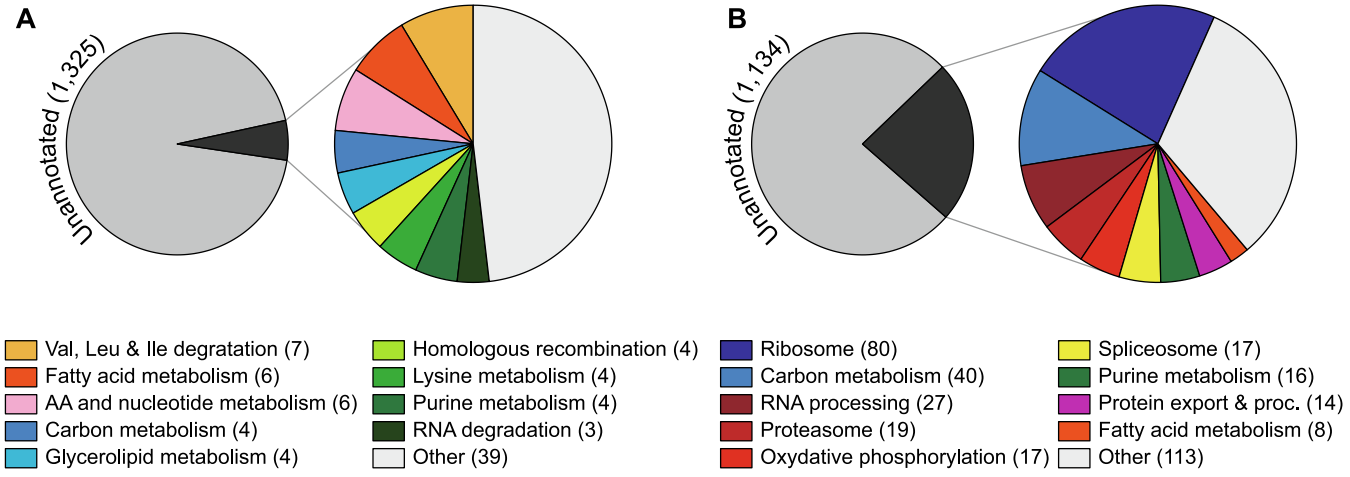

Fig. 1. Classification summary of annotated genes differentially expressed for *T. pseudonana* acclimated to growth under low and high constant light conditions using the fold change threshold > 2, $p < 0.05$. (A) Annotations of genes down-regulated in low light acclimated (i.e., slow-growing) cells. (B) Annotations of genes up-regulated in low light acclimated cells. Numbers in parentheses represent the number of significantly expressed genes with annotations in the KEGG database. (For interpretation of the references to color in this figure legend, the reader is referred to the web version of this article.)

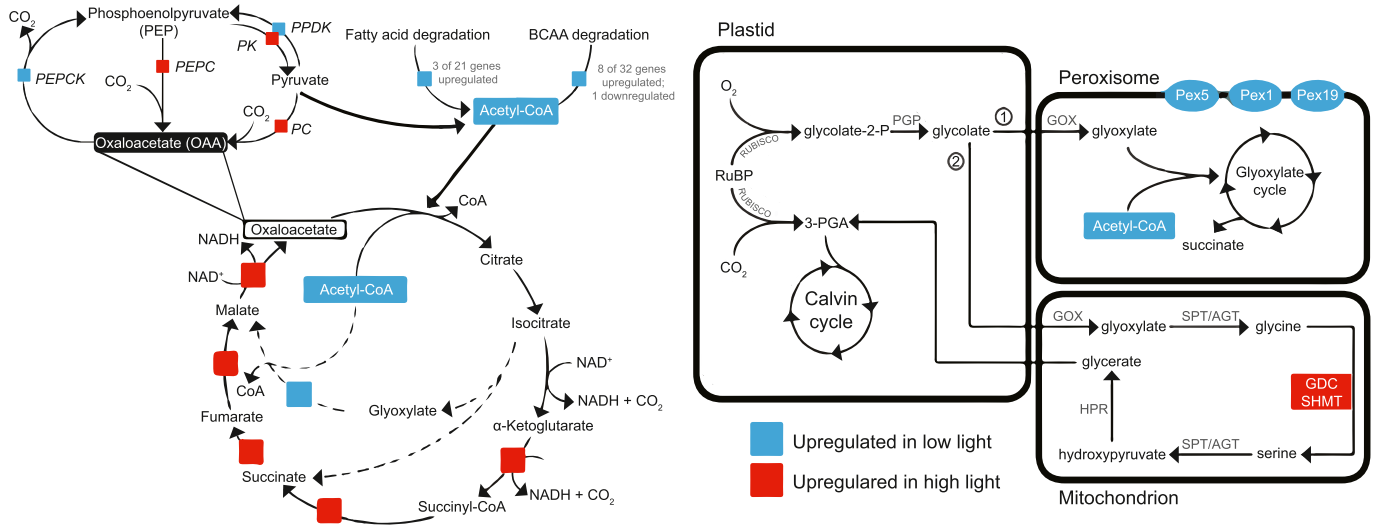

Fig. 2. Metabolite pathway visualization of differentially expressed genes for *T. pseudonana* at constant high (200 μmol photons m^{-2} s^{-1}) and low (5 μmol photons m^{-2} s^{-1}) light. Genes that were upregulated in high light are represented in red, genes that were upregulated in low light acclimated cells are represented in blue. Right panel figure shows the interplay between processes occurring in the plastid, peroxisome and mitochondrion. Left panel figure shows more detailed interactions between glycolysis, fatty acid and branched chain amino acid (BCAA) degradation and TCA cycle where dashed black lines represent the glyoxylate cycle two-step bypass. PEPCK = phosphoenolpyruvate (PEP) carboxykinase; PPDK = pyruvate-phosphate dikinase; PK = pyruvate kinase; PC = pyruvate carboxylase; PEPC = PEP carboxylase; OAA = oxaloacetate; BCAA = branched chain amino acid; Pex1/5/19 = genes for various peroxins that import proteins into the peroxisome; GDC = glycine decarboxylase; SHMT = serine hydroxymethyltransferase. Fold changes and *p* values for these genes are displayed in Table S5. (For interpretation of the references to color in this figure legend, the reader is referred to the web version of this article.)

PLS-DA (Fig. 3C) plots. The distribution of samples from high (HC) and low (LC) constant light treatments did not overlap with one another, but both overlapped with the medium (MC) constant light, and together 38.2 % and 21.5 % of this variation was explained by PC1 and PC2, respectively (Fig. 3A). High (HP) and low (LP) pulse light treatments exhibited a slight overlap, with variation by PC1 and PC2 explained by 56 and 22.3 %, respectively (Fig. 3B). Directly comparing the high and low light intensities for constant (HC, LC) and pulse (HP, LP) treatments revealed less distinct clusters via PCA (Fig. S1). However, PLS-DA analysis (Fig. 3C) revealed spatial separation along 4 components (Q^2 = 0.861), which suggests light intensity affected the metabolite profiles, although larger sample sizes are required to validate the classification model fit (10-fold cross-validation; p = 0.155). These data show that light intensity exerts a greater influence on the metabolite pool than light regime (i.e., total daily integrated photon dose).

Significant differences in metabolic profiles within and between light treatments were identified using SAM, supplemented by post-hoc comparisons via ANOVA and Tukey's tests. We identified 9 metabolites that were significantly different within the constant light treatments (HC, MC, LC), whereby metabolite upregulation (i.e., higher relative concentration) varied between light intensities (Fig. 4). The metabolites identified were phytol, dihydroxybutyric acid (C4:1), eicosanoic acid (C20:0), threonic acid, furoic acid, fructose, aspartate, glyceryl-glycoside and lactate (Fig. 4). Phytol, C20:0 and glyceryl-glycoside were more abundant at mid-lower (MC, LC) light intensities, C4:1 and fructose were more abundant at mid-higher (MC, HC) light intensities. Threonic acid (10.7-fold), furoic acid (3.7-fold), aspartate (2.1-fold) and lactate (2.5-fold) were, specifically, more abundant in HC treatments compared to LC treatments (Fig. 4). Notably, there was a 10.7-fold increase in C20:0 and 6.9-fold increase in phytol in LC compared to HC treatments. In the pulse light dose treatments (LP, HP), 11 metabolites significantly varied in relative abundance with light intensity (Fig. 4). Some of these metabolites were observed in both constant and pulse light treatments (e.g., C4:1, lactate, fructose, threonic acid, aspartate), but some metabolites were unique to pulse light dose treatments (e.g., arabinose, succinate, pentanoic acid (C5:0), myristic acid (C14:0), cycloartenol and anthraquinone) (Fig. 4) highlighting a potential diurnal effect on metabolic profiles. Of these, cycloartenol and anthraquinone had the greatest change, with a 19.8-fold and 8.1-fold increase, respectively, in HP compared to LP treatments.

SAM-generated inter-comparisons between light treatments of equal average PFD but varying light dose (HC, HP, LC, LP) identified 19 metabolites that significantly differed in relative abundance (Fig. 4). These significant metabolites showed similar relationships to light intensity, including the 9 metabolites identified for the constant light intra-comparison (i.e., LC, MC, HC) except glyceryl-glycoside, as well as the 11 metabolites identified for pulse light intra-comparison (LP, HP), except succinate (Fig. 4). Despite the aforementioned metabolite repeats, the inter-comparison of light treatments of equal average PFD did reveal six new significant metabolites: scyllo-inositol, ribose, trehalose, glucose, glycolic acid and butanoic acid (C4:0) (Fig. 4). Separating light dose treatments by light intensity highlighted that between low light intensity treatments, LC appeared to have larger pools of all significant metabolites identified compared to LP, with the largest fold changes in fructose (5.6-fold), trehalose (5.5-fold), cylcoartenol (4.9-fold), scyllo-inositol (3.9-fold) and phytol (3.3-fold) (Fig. 4). Whereas at high light intensities, 15 of the 19 significant metabolites were present in higher amounts in HC compared to HP, including trehalose (4.3-fold), fructose (3.1-fold), scyllo-inositol (2.5-fold), and threonic acid (2.4-fold) (Fig. 4).

Overall, lactate, aspartate, C4:1, fructose and threonic acid were the only metabolites that were statistically different for all comparisons of light intensity and light dose (Fig. 4). When comparing constant and pulse high and low light treatments, some metabolites were found to be exclusively significant on the basis of light intensity whereby lactate, C5:0 and ribose were consistently present at higher abundance at high light intensities while C20:0 and phytol were more abundant at low light intensities. Light intensity appeared to influence the metabolites identified as significant, but the relative abundances of those metabolites were seemingly more impacted by light dose (Fig. 5). Specifically, 13 of the metabolites identified using SAM were significant because of light intensity irrespective of dose and only two (C4:0 and scyllo-inositol) were driven by light dose (Fig. 4).

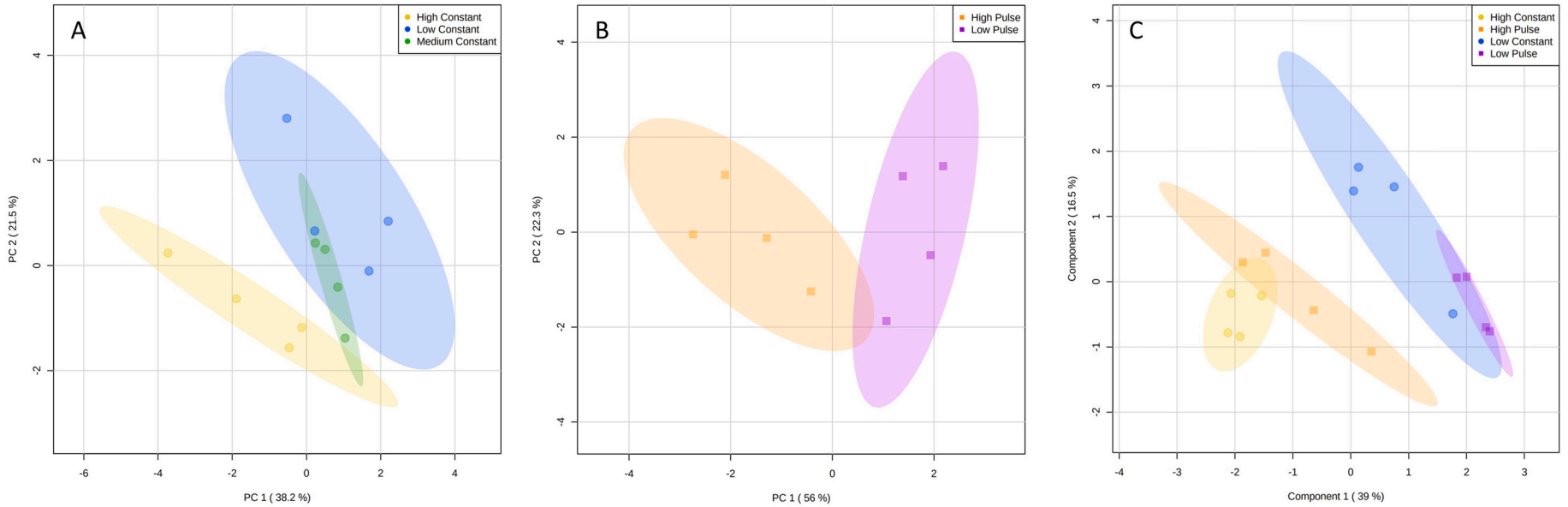

Fig. 3. Metabolite profiles grouped according to light treatments. (A) PCA of relative metabolite abundances for constant light treatments (24:0 L:D) at high (yellow circles), medium (green circles) and low (blue circles) intensities. (B) PCA of relative metabolite abundances for pulse (12:12 L:D) light treatments at high (orange squares) and low (purple squares) intensities. (C) PLS-DA of relative metabolite abundances for constant and pulse light treatments at high and low light intensities to combine light intensity and light dose treatments with equal average PFD. Shaded areas represent the 95 % confidence region of individual treatment groups. Individual data points represent independent biological replicates (n = 4). (For interpretation of the references to color in this figure legend, the reader is referred to the web version of this article.)

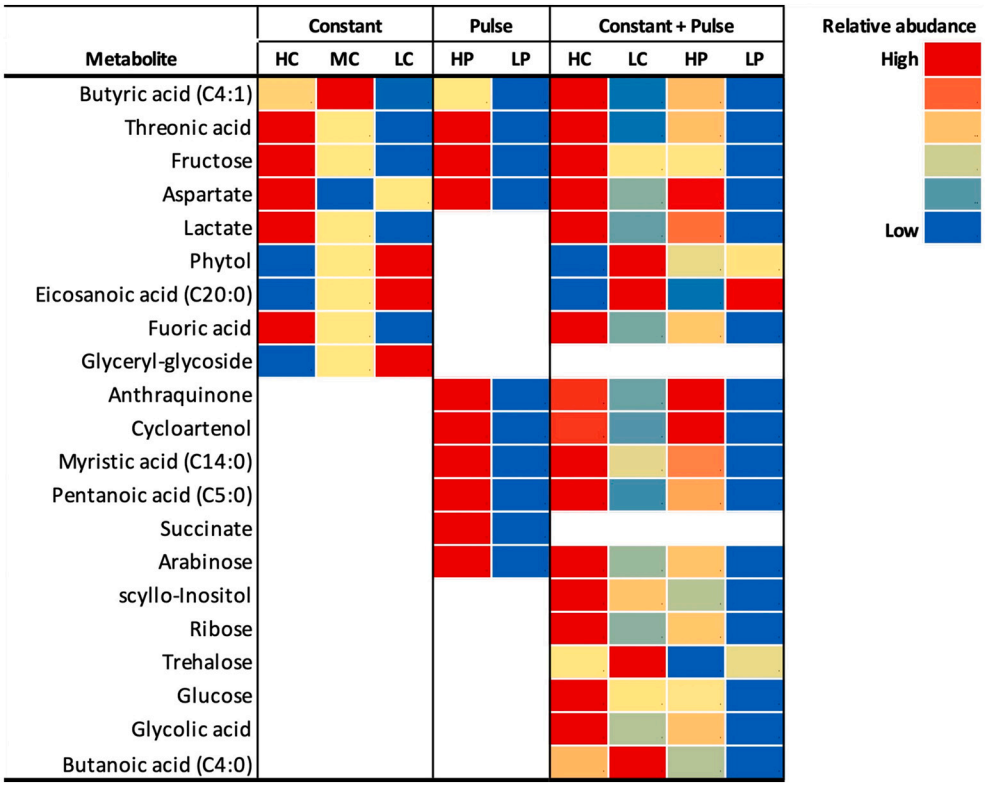

Fig. 4. Heatmap showing the compilation of metabolites identified as significantly different by SAM for the various comparisons of light treatments – constant, pulse and constant+pulse treatments of equal average PFD. Significant differences ($p_{adj} < 0.05$) in metabolite relative abundance between light treatments are represented using shades of blue for lower relative abundance and shades of red for higher relative abundance. A lack of significant difference is represented by yellow. (For interpretation of the references to color in this figure legend, the reader is referred to the web version of this article.)

4. Discussion

Light-driven differences in metabolite profiles coupled with gene expression patterns revealed metabolic re-adjustments required to maintain energy and carbon flux under wide ranging light conditions. Metabolites involved with glycolysis and the synthesis of fatty acids and carbohydrates were indicative of cells capable of high energy and carbon investments supporting the observed rapid growth in high light (Figs. 5, 6). Metabolites associated with gluconeogenesis and energy storage were detected in higher amounts in slow growing, low-light acclimated cells, but the low retrieval of metabolites in these cells suggested that their metabolic pools were rapidly turned over with few luxury stores. In our experiments, where cells were in balanced growth, metabolite detection indicated that metabolite pools were (1) being actively produced in high quantities to meet cellular demand or (2) used at a slower rate than the consumption rate (i.e., had a slow turnover rate) under the experimental condition. The combined metabolomic and gene expression data show that the observed 6.5- to 7-fold change in light-driven growth rate is facilitated by key pathway gating strategies that result in shifts in carbon and energy flux. Below, the metabolic strategies that emerged from our analyses are described and include light harvesting through glycolysis and central carbon metabolism.

4.1. Light harvesting

Higher amounts of pigment-associated metabolites in low light relative to high light treatments is attributed to photoacclimation, a generalized phytoplankton behavior whereby light absorption is increased under light limitation to fuel downstream carbon fixation (Table 1) [63]. Photoacclimation is evidenced by the 1.7-fold increase of Chl *a* cell^{-1} under LC and the 6.9-fold increase in phytol, a constituent of Chl *a* [91]. In addition, higher concentrations of long chain polyunsaturated fatty acids (e.g., oleic acid (C18:1n9) and docosahexaenoic acid (C22:6n3)) were observed in low light treatments, suggesting active turnover of membrane lipids, or alternatively, a storage pool of long-lived energy available to slow growing cells [92]. The 10.7-fold increase of the signalling molecule eicosanoic acid (C20:0) in low light cells suggests a preparatory activity associated with diatoms' rapid responses to dynamic light [93]. If C20:0 poises diatoms to sense minute changes in light availability, this mechanism could help explain the ability of these cells to exhibit an unusually wide range of light-dependent growth rates [94]. Alternatively, the presence of C20:0 under low light could indicate accumulation and slow turnover of this compound in the cellular matrix.

4.2. Gating carbon flux through the glycolysis - gluconeogenesis hub

Glycolysis/gluconeogenesis extend across multiple compartments in diatoms including the cytosol, chloroplast and mitochondria [95]. Glycolysis generates energy (ATP) and pyruvate, while gluconeogenesis works in opposition to glycolysis to produce carbohydrates and energy storage molecules. The 6- to 7-fold upregulation of genes encoding *PDK1_2* (localized to the cytosol [96]) and *PCK1* (localized to the mitochondria [96]) in low light is consistent with the larger pools of the gluconeogenesis end-product trehalose (5.5-fold increase) in low-light acclimated cells [97–99] (Fig. 5). *PDK1_2* and *PCK1* are enzymes in a critical hub for diatom carbon flux regulation [96]. Upregulation of these key enzymes will increase flux through gluconeogenesis and away from glycolysis by catalyzing the conversion of pyruvate and oxaloacetate (OAA) to phosphoenolpyruvate (PEP) (Table S5; Fig. 2). In slower growing cells, increasing flux through this critical hub appears to limit energy and carbon loss to rapid glycolytic activity. During light limited growth, low carbon fixation rates and rapid turnover of newly fixed carbon require careful tuning of carbon flux mechanisms to prevent carbon depletion [19].

The combined omics approaches used here and applied to cells fully acclimated to their light environment indicate that central carbon metabolism is tightly regulated at the level of transcription, such that metabolites including pyruvate, OAA and PEP have rapid turnover rates, preventing their detection by GC–MS. Specifically, our GC–MS method

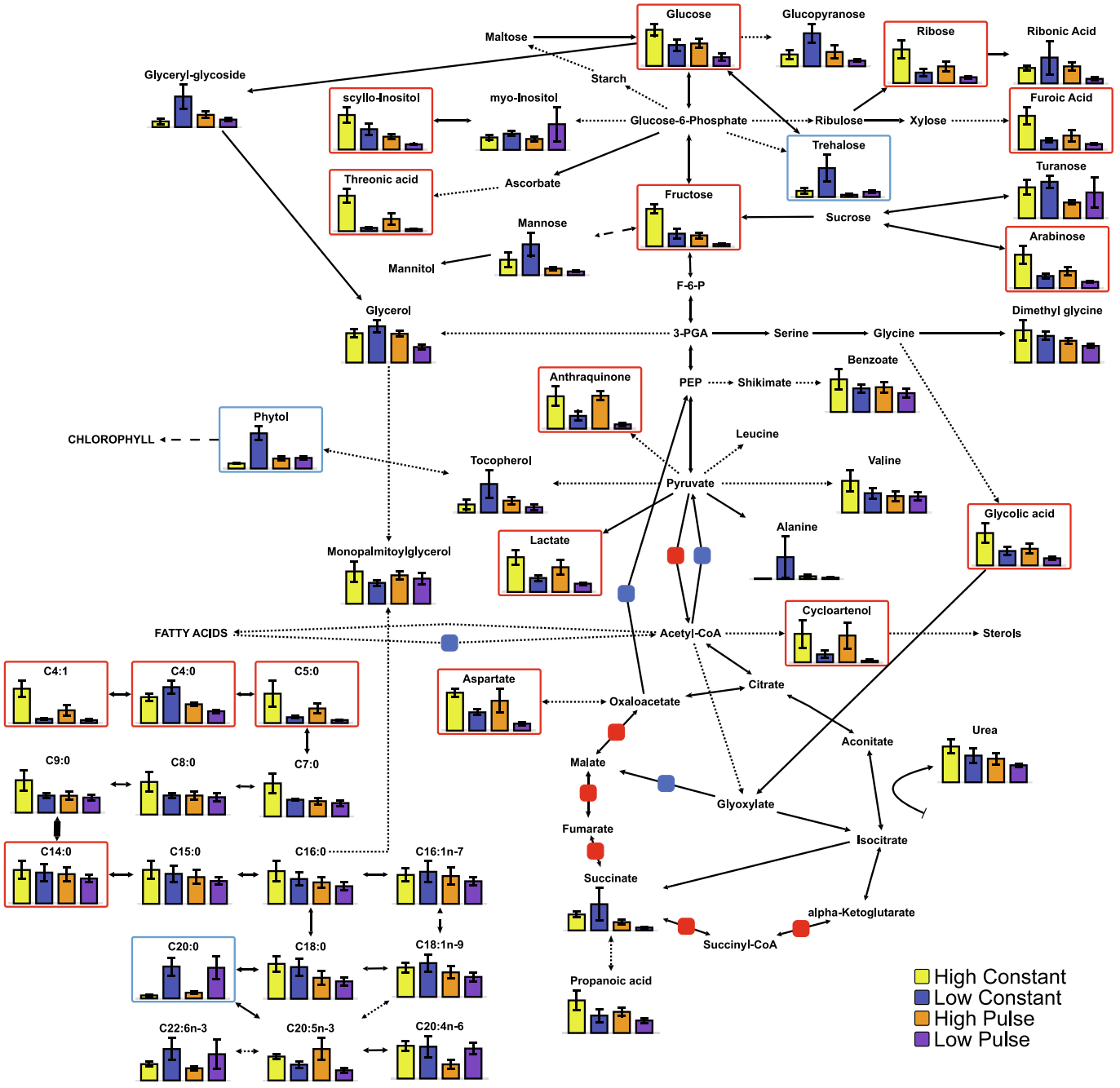

Fig. 5. Metabolite pathway visualization of relative metabolite concentrations for *T. pseudonana* grown under constant (24:0 L:D) and pulse (12:12 L:D) light dose at low (5 μmol photons m^{-2} s^{-1}) and high (200 μmol photons m^{-2} s^{-1}) light intensities. Identified metabolites from GC–MS are distinguished with a graph of relative metabolite concentrations. Dashed black lines signify metabolites that are indirectly connected and solid black lines show cellular processes that are directly connected. Metabolites outlined with red frames represent significant metabolites found in higher relative abundance under high light and metabolites outlined with blue frames represent significant metabolites found in higher relative abundance under low light. Solid squares represent some significant genes that were found to be upregulated in high light (red) or upregulated in low light (blue) treatments (see Fig. 2 for more detailed gene expression data). (For interpretation of the references to color in this figure legend, the reader is referred to the web version of this article.)

was not able to detect pyruvate [84] or OAA and PEP detection had not yet been attempted. In contrast, gene expression facilitates accumulation of some end-product metabolites that are important in maintaining cell viability in very low light. Unbalanced growth may cause periodic accumulation of pyruvate, OAA and PEP, as well as other metabolites not observed in our experiments studying cells in balanced growth.

4.3. Pyruvate and acetyl-CoA

Lactate fermentation appears to play an important role in maintaining sufficient NAD^+ to facilitate ongoing pyruvate oxidation and an uninterrupted TCA cycle [100]. Glycolysis yields pyruvate, which can be fermented to lactate or converted to acetyl CoA or OAA. The latter two compounds enter the TCA cycle in the mitochondria [99]. High-light acclimated cells contained higher concentrations of cycloartenol (19.8-fold increase between LP and HP, and 3.6-fold increase between

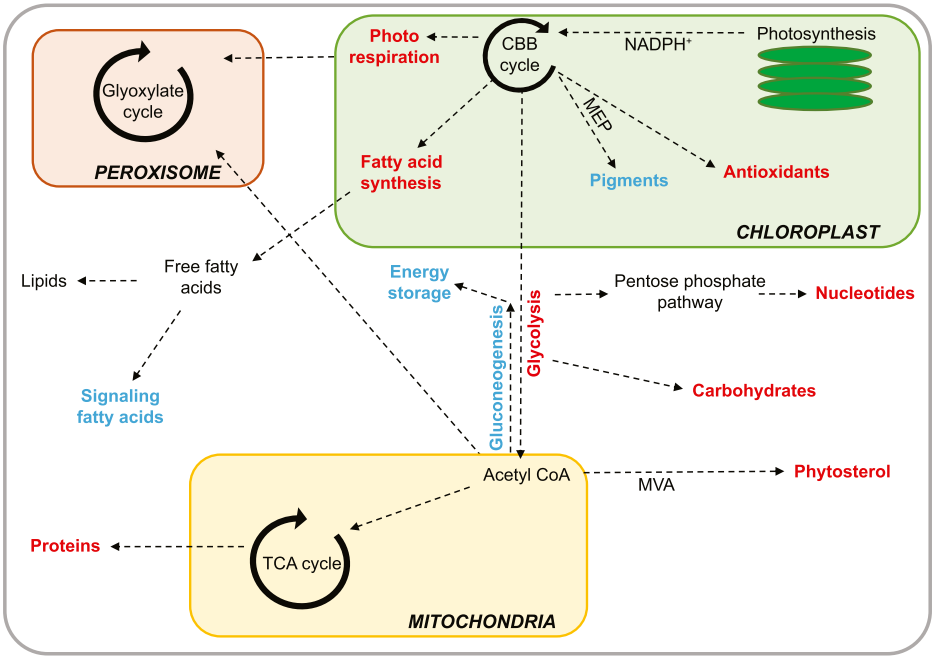

Associated significant metabolites upregulated under high/low light	
Photorespiration	Glycolic Acid
Pigments	Phytol
Antioxidants	Anthraquinone
Fatty acid synthesis	C14:0, C4:0, C4:1, C5:0
Signaling fatty acids	Eicosanoic acid (C20:0)
Glycolysis	Glucose, fructose, lactate
Carbohydrates	Arabinose, furoic acid, threonic acid, scyllo-inositol
Gluconeogenesis, energy storage	Trehalose
Proteins	Aspartate
Nucleotides	Ribose
Phytosterol	Cycloartenol

Fig. 6. Schematic of identified significant metabolic changes in *T. pseudonana* grown under high vs low light intensity for both constant and pulse light treatments. Color type indicates upregulation (blue) and downregulation (red) of relative metabolite concentrations for corresponding processes under lower light acclimation. Black dashed arrows indicate intermediary steps/processes that were not significantly up or down regulated according to the metabolites identified across all light treatments. Abbreviations: CBB cycle – Calvin-Benson-Bassham cycle; TCA cycle – tricarboxylic acid cycle; MVA - mevalonate pathway; MEP – methylerythritol phosphate pathway. (For interpretation of the references to color in this figure legend, the reader is referred to the web version of this article.)

LC and HC), an essential structural cell membrane phytosterol, that supports rapid cell division [101–103] (Fig. 5). Lactate accumulation in high light treatments indicates that lactate fermentation induced by high rates of oxygen respiration is used to regenerate NAD^+ needed to oxidize TCA cycle intermediates [104] and was also observed under nutrient limitation in *T. pseudonana* [105].

4.4. The glyoxylate cycle conserves carbon in light limited cells

The glyoxylate cycle and photorespiration also function to prevent carbon depletion in light limited cells. The glyoxylate cycle is a truncated version of the TCA cycle that operates in the peroxisome and does not produce CO_2 [106]. CO_2 conservation is achieved via a two-step bypass. In the first step, isocitrate lyase converts isocitrate to succinate and glyoxylate; in the second step, malate synthase (upregulated in low light cells) condenses glyoxylate and acetyl-CoA to form malate. Malate can replenish the glyoxylate cycle through the action of malate dehydrogenase, and succinate can be used to replenish the TCA cycle or serve as precursors for carbohydrate or amino acid biosynthesis [107]. Three genes encoding peroxin (Pex) transporters were upregulated in low light relative to high light (Fig. 2), supporting the increased transport of substrates fuelling the glyoxylate cycle: acetyl-CoA and isocitrate [108,109]. The branched-chain amino acid (BCAA) and fatty acid degradation pathways upregulated in low light provide a reliable source of acetyl-CoA to feed the glyoxylate cycle in the peroxisome and the TCA cycle in the mitochondria.

All of the genes encoding enzymes involved in TCA cycle reactions that are bypassed by the glyoxylate cycle were downregulated in low light cells with the exception of isocitrate dehydrogenase, probably because it is needed to maintain production of reducing equivalents (NADH) and α-ketoglutarate, a key precursor for amino acid synthesis.

Fast growing cells require a high functioning TCA cycle to support energy requirements and amino acid and nucleotide precursors for biosynthesis and growth. Faster growing, high light cells exhibit lower C:N than low light cells (Table 1), a property driven by high cellular nitrogen. C:N is associated with the positive relationship between ribosome content and growth rate [110,111]. Aspartate derived from OAA was present in significantly higher amounts in high light acclimated cells. Succinate was retrieved in the *T. pseudonana* metabolite profile, but was not detected in significantly different concentrations between light treatments. Nevertheless, the role of succinate as a fundamental intermediate in the glyoxylate and TCA cycles, as well as redox-shuttling between the cytosol and peroxisome, warrants further study, possibly by flux-based analysis, which may help elucidate its regulatory role in growth rate modulation.

In high light, photorespiration is inevitable, but cells have adapted strategies to use this pathway in a beneficial way. Photorespiration produces glycolic acid via oxygenase activity of RuBisCO. Glycolic acid and genes encoding photorespiratory enzymes (GDC and SHMT) were retrieved in greater amounts in high light compared to low light cells, consistent with higher rates of photorespiration with irradiance [112,113]. We propose that photorespiratory-generated glycolic acid under high light is initially repurposed in the mitochondria to prevent chloroplastic damage from overreduction, rather than immediately returned to the CBB cycle, thus allowing simultaneous dissipation of energy and repurposing of carbon skeletons [44,114]. Glycolic acid has been proposed to have an important role in maintaining cellular energy balance [44], especially in conditions where rapidly growing cells are balancing demands for ATP synthesis via respiration with needs for reduced nucleotides for biosynthesis.

5. Conclusion

The differences we observed in metabolite abundances depending on light dose show that cells adjust metabolic pathways to accommodate light and dark periods and demonstrate the extraordinary metabolic plasticity used to optimize growth in dynamic light environments. Our study integrates “omics” data in a novel way yielding new insights into growth strategies for the model diatom, *T. pseudonana*. We expect that some pathway gating mechanisms, such as the heavy reliance on

peroxisomal glyoxylate cycling in low light, are specialized to diatoms, but other mechanisms, especially the glycolysis – gluconeogenesis hub, operate across phytoplankton groups. This study demonstrates the power of combined metabolite and gene profiling for unlocking "emergent" physiologies that are shared across phytoplankton groups and that can be used to understand broad scale growth and productivity and leveraged for bio-production purposes.

Funding

NLF was supported by the UTS International Research Scholarship and President's Scholarship. JLM was supported by a Human Frontier Science Programme Long-term Postdoctoral fellowship (LT000625/2018-L).

CRediT authorship contribution statement

NLF, KHH, DJS and PJR designed the study; NLF performed the experiments. JBR assisted the metabolite extraction and supplies. NLF, MP, EMS and JLM analyzed the data; NLF, KHH, DJS, JLM wrote the article with contributions from JBR, MP, PJR, AL and EMS.

Declaration of competing interest

The authors declare that they have no known competing financial interests or personal relationships that could have appeared to influence the work reported in this paper.

Data availability

All data are available within the paper and supplementary materials published online. All RNAseq data deposited to NCBI (BioProject PRJNA976330), metabolite data to Zenodo (10.5281/zenodo.7803966).

Acknowledgements

The authors acknowledge N. Jayasinghe (Metabolomics Australia, University of Melbourne) for advice on extracting metabolomics samples and Samantha Bennett for help with culture maintenance.

Appendix A. Supplementary data

Supplementary data to this article can be found online at https://doi.org/10.1016/j.algal.2023.103172.

References

[1] P. Tréguer, D.M. Nelson, A.J. Van Bennekom, D.J. Demaster, A. Leynaert, B. Quéguiner, The silica balance in the world ocean: a reestimate, Science 268 (5209) (1995) 375–379, https://doi.org/10.1126/science.268.5209.375.
[2] R.J. Geider, E.H. Delucia, P.G. Falkowski, A.C. Finzi, J. Philip Grime, J. Grace, F. Ian Woodward, Primary productivity of planet earth: biological determinants and physical constraints in terrestrial and aquatic habitats, Glob. Chang. Biol. 7 (8) (2001) 849–882, https://doi.org/10.1046/j.1365-2486.2001.00448.x.
[3] E.V. Armbrust, The life of diatoms in the world's oceans, Nature 459 (7244) (2009) 185–192, https://doi.org/10.1038/nature08057.
[4] D.G. Mann, P. Vanormelingen, An inordinate fondness? The number, distributions, and origins of diatom species, J. Eukaryot. Microbiol. 60 (4) (2013) 414–420, https://doi.org/10.1111/jeu.12047.
[5] K. Richardson, J. Beardall, J.A. Raven, Adaptation of unicellular algae to irradiance: an analysis of strategies, New Phytol. 93 (2) (1983) 157–191, https://doi.org/10.1111/j.1469-8137.1983.tb03422.x.
[6] H.L. Macintyre, T.M. Kana, R.J. Geider, The effect of water motion on short-term rates of photosynthesis by marine phytoplankton, Trends Plant Sci. 5 (1) (2000) 12–17, https://doi.org/10.1016/S1360-1385(99)01504-6.
[7] S. Tozzi, O. Schofield, P. Falkowski, Historical climate change and ocean turbulence as selective agents for two key phytoplankton functional groups, Mar. Ecol. Prog. Ser. 274 (Raven 1997) (2004) 123–132, https://doi.org/10.3354/meps274123.
[8] M.J. Behrenfeld, E.S. Boss, Resurrecting the ecological underpinnings of ocean plankton blooms, Annu. Rev. Mar. Sci. 6 (1) (2014) 167–194, https://doi.org/10.1146/annurev-marine-052913-021325.
[9] M.J. Behrenfeld, K. Worthington, R.M. Sherrell, F.P. Chavez, P. Strutton, M. McPhaden, D.M. Shea, Controls on tropical Pacific Ocean productivity revealed through nutrient stress diagnostics, Nature 442 (7106) (2006) 1025–1028, https://doi.org/10.1038/nature05083.
[10] G. Kulk, W.H. van de Poll, R.J.W. Visser, A.G.J. Buma, Low nutrient availability reduces high-irradiance-induced viability loss in oceanic phytoplankton, Limnol. Oceanogr. 58 (5) (2013) 1747–1760, https://doi.org/10.4319/lo.2013.58.5.1747.
[11] D.J. Hughes, D. Varkey, M.A. Doblin, T. Ingleton, A. Mcinnes, P.J. Ralph, D. J. Suggett, Impact of nitrogen availability upon the electron requirement for carbon fixation in Australian coastal phytoplankton communities, Limnol. Oceanogr. 63 (5) (2018) 1891–1910, https://doi.org/10.1002/lno.10814.
[12] H.M. Van Tol, E.V. Armbrust, Genome-scale metabolic model of the diatom *Thalassiosira pseudonana* highlights the importance of nitrogen and sulfur metabolism in redox balance, PLoS One 16 (3) (2021), e0241960, https://doi.org/10.1371/journal.pone.0241960.
[13] J. Lavaud, R.F. Strzepek, P.G. Kroth, Photoprotection capacity differs among diatoms: possible consequences on the spatial distribution of diatoms related to fluctuations in the underwater light climate, Limnol. Oceanogr. 52 (3) (2007) 1188–1194, https://doi.org/10.2307/4499689.
[14] J. Park, F.I. Kuzminov, B. Bailleul, E.J. Yang, S.H. Lee, P.G. Falkowski, M. Y. Gorbunov, Light availability rather than Fe controls the magnitude of massive phytoplankton bloom in the Amundsen Sea polynyas, Antarctica, Limnol. Oceanogr. 62 (5) (2017) 2260–2276, https://doi.org/10.1002/lno.10565.
[15] H. Wagner, T. Jakob, C. Wilhelm, Balancing the energy flow from captured light to biomass under fluctuating light conditions, New Phytol. 169 (1) (2006) 95–108, https://doi.org/10.1111/j.1469-8137.2005.01550.x.
[16] T. Jakob, H. Wagner, K. Stehfest, C. Wilhelm, A complete energy balance from photons to new biomass reveals a light- and nutrient-dependent variability in the metabolic costs of carbon assimilation, J. Exp. Bot. 58 (8) (2007) 2101–2112, https://doi.org/10.1093/jxb/erm084.
[17] C. Wilhelm, T. Jakob, From photons to biomass and biofuels: evaluation of different strategies for the improvement of algal biotechnology based on comparative energy balances, Appl. Microbiol. Biotechnol. 92 (5) (2011) 909–919, https://doi.org/10.1007/s00253-011-3627-2.
[18] K.H. Halsey, B.M. Jones, Phytoplankton strategies for photosynthetic energy allocation, Annu. Rev. Mar. Sci. 7 (1) (2015) 265–297, https://doi.org/10.1146/annurev-marine-010814-015813.
[19] N.L. Fisher, K.H. Halsey, Mechanisms that increase the growth efficiency of diatoms in low light, Photosynth. Res. 129 (2) (2016) 183–197, https://doi.org/10.1007/s11120-016-0282-6.
[20] H. Wagner, T. Jakob, A. Fanesi, C. Wilhelm, Towards an understanding of the molecular regulation of carbon allocation in diatoms: the interaction of energy and carbon allocation, Philos. Trans. Royal Soc. B: Biol. Sci. 372 (1728) (2017), https://doi.org/10.1098/rstb.2016.0410.
[21] C.M. Moore, D.J. Suggett, A.E. Hickman, Y.-N. Kim, J.F. Tweddle, J. Sharples, P. M. Holligan, Phytoplankton photoacclimation and photoadaptation in response to environmental gradients in a shelf sea, Limnol. Oceanogr. 51 (2) (2006) 936–949. Retrieved from, https://aslopubs.onlinelibrary.wiley.com/doi/pdf/10.4319/lo.2006.51.2.0936. Retrieved from.
[22] M.J. Behrenfeld, T.K. Westberry, E.S. Boss, R.T. O'Malley, D.A. Siegel, Satellite-detected fluorescence reveals global physiology of ocean phytoplankton, Biogeosciences 6 (5) (2009) 779–794, https://doi.org/10.5194/bg-6-779-2009.
[23] D.J. Suggett, C.M. Moore, A.E. Hickman, R.J. Geider, Interpretation of fast repetition rate (FRR) fluorescence: signatures of phytoplankton community structure versus physiological state, Mar. Ecol. Prog. Ser. 376 (2009) 1–19, https://doi.org/10.3354/meps07830.
[24] D.J. Suggett, C.M. Moore, R.J. Geider, Chlorophyll a fluorescence in aquatic sciences: methods and application, in: Chlorophyll a Fluorescence in Aquatic Sciences: Methods and Applications, 2010, https://doi.org/10.1007/978-90-481-9268-7.
[25] G.M. Silsbe, R.E.H. Smith, M.R. Twiss, Quantum efficiency of phytoplankton photochemistry measured continuously across gradients of nutrients and biomass in Lake Erie (Canada and USA) is strongly regulated by light but not by nutrient deficiency, Can. J. Fish. Aquat. Sci. 72 (5) (2015) 651–660, https://doi.org/10.1139/cjfas-2014-0365.
[26] G.M. Silsbe, M.J. Behrenfeld, K.H. Halsey, A.J. Milligan, T.K. Westberry, The CAFE model: a net production model for global ocean phytoplankton, Glob. Biogeochem. Cycles 30 (12) (2016) 1756–1777, https://doi.org/10.1002/2016GB005521.
[27] G. Li, D.A. Campbell, Rising CO_2 interacts with growth light and growth rate to alter photosystem II photoinactivation of the coastal diatom *Thalassiosira pseudonana*, PLoS One 8 (1) (2013), https://doi.org/10.1371/journal.pone.0055562.
[28] G. Li, A.D. Woroch, N.A. Donaher, A.M. Cockshutt, D.A. Campbell, A hard day's night: diatoms continue recycling photosystem II in the dark, Front. Mar. Sci. 3 (November) (2016) 1–10, https://doi.org/10.3389/fmars.2016.00218.
[29] R. Zhang, Z. Kong, S. Chen, Z. Ran, M. Ye, J. Xu, X. Yan, The comparative study for physiological and biochemical mechanisms of *Thalassiosira pseudonana* and *Chaetoceros calcitrans* in response to different light intensities, Algal Res. 27 (April) (2017) 89–98, https://doi.org/10.1016/j.algal.2017.08.026.
[30] N.L. Fisher, D.A. Campbell, D.J. Hughes, U. Kuzhiumparambil, K.H. Halsey, P. J. Ralph, D.J. Suggett, Divergence of photosynthetic strategies amongst marine

diatoms, PLoS One 15 (12) (2020) 1–27, https://doi.org/10.1371/journal.pone.0244252.
[31] D.J.S. Montagnes, D.J. Franklin, Effect of temperature on diatom volume, growth rate, and carbon and nitrogen content: reconsidering some paradigms, Limnol. Oceanogr. 46 (8) (2001) 2008–2018, https://doi.org/10.4319/lo.2002.47.4.1272.
[32] K.H. Halsey, A.J. Milligan, M.J. Behrenfeld, Linking time-dependent carbon-fixation efficiencies in *Dunaliella tertiolecta* (Chlorophyceae) to underlying metabolic pathways, J. Phycol. 47 (1) (2011) 66–76, https://doi.org/10.1111/j.1529-8817.2010.00945.x.
[33] K.H. Halsey, R.T. O'Malley, J.R. Graff, A.J. Milligan, M.J. Behrenfeld, A common partitioning strategy for photosynthetic products in evolutionarily distinct phytoplankton species, New Phytol. 198 (4) (2013) 1030–1038, https://doi.org/10.1111/nph.12209.
[34] K. Halsey, A. Milligan, M. Behrenfeld, Contrasting strategies of photosynthetic energy utilization drive lifestyle strategies in ecologically important picoeukaryotes, Metabolites 4 (2) (2014) 260–280, https://doi.org/10.3390/metabo4020260.
[35] A. Montsant, A.E. Allen, S. Coesel, A. De Martino, A. Falciatore, M. Mangogna, C. Bowler, Identification and comparative genomic analysis of signaling and regulatory components in the diatom *Thalassiosira pseudonana*, J. Phycol. 43 (3) (2007) 585–604, https://doi.org/10.1111/j.1529-8817.2007.00342.x.
[36] T.I. McLean, "Eco-omics": a review of the application of genomics, transcriptomics, and proteomics for the study of the ecology of harmful algae, Microb. Ecol. 65 (4) (2013) 901–915, https://doi.org/10.1007/s00248-013-0220-5.
[37] J. Levering, C.L. Dupont, A.E. Allen, B.O. Palsson, K. Zengler, Integrated regulatory and metabolic networks of the marine diatom *Phaeodactylum tricornutum* predict the response to rising CO_2 levels, MSystems 2 (1) (2017) 1–12, https://doi.org/10.1128/msystems.00142-16.
[38] S.A. Amin, L.R. Hmelo, H.M. Van Tol, B.P. Durham, L.T. Carlson, K.R. Heal, E. V. Armbrust, Interaction and signalling between a cosmopolitan phytoplankton and associated bacteria, Nature 522 (7554) (2015) 98–101, https://doi.org/10.1038/nature14488.
[39] W.M. Johnson, M.C. Kido Soule, E.B. Kujawinski, Evidence for quorum sensing and differential metabolite production by a marine bacterium in response to DMSP, ISME J. 10 (9) (2016) 2304–2316, https://doi.org/10.1038/ismej.2016.6.
[40] S.R. Smith, C.L. Dupont, J.K. McCarthy, J.T. Broddrick, M. Oborník, A. Horák, A. E. Allen, Evolution and regulation of nitrogen flux through compartmentalized metabolic networks in a marine diatom, Nat. Commun. 10 (1) (2019), https://doi.org/10.1038/s41467-019-12407-y.
[41] J. Ashworth, S. Coesel, A. Lee, E.V. Armbrust, M.V. Orellana, N.S. Baliga, Genome-wide diel growth state transitions in the diatom *Thalassiosira pseudonana*, Proc. Natl. Acad. Sci. U. S. A. 110 (18) (2013) 7518–7523, https://doi.org/10.1073/pnas.1300962110.
[42] J. Ashworth, S. Turkarslan, M. Harris, M.V. Orellana, N.S. Baliga, Pan-transcriptomic analysis identifies coordinated and orthologous functional modules in the diatoms *Thalassiosira pseudonana* and *Phaeodactylum tricornutum*, Mar. Genomics 26 (2016) 21–28, https://doi.org/10.1016/j.margen.2015.10.011.
[43] S.R. Smith, J.T. Gillard, A.B. Kustka, J.P. McCrow, J.H. Badger, H. Zheng, A. E. Allen, Transcriptional orchestration of the global cellular response of a model pennate diatom to diel light cycling under iron limitation, PLoS Genet. 12 (12) (2016), e1006490.
[44] A. Davis, R. Abbriano, S.R. Smith, M. Hildebrand, Clarification of photorespiratory processes and the role of malic enzyme in diatoms, Ann. Anat. 168 (1) (2017) 134–153, https://doi.org/10.1016/j.protis.2016.10.005.
[45] N.R. Cohen, W. Gong, D.M. Moran, M.R. McIlvin, M.A. Saito, A. Marchetti, Transcriptomic and proteomic responses of the oceanic diatom *Pseudo-nitzschia granii* to iron limitation, Environ. Microbiol. 20 (8) (2018) 3109–3126, https://doi.org/10.1111/1462-2920.14386.
[46] S.T. Dyhrman, B.D. Jenkins, T.A. Rynearson, M.A. Saito, M.L. Mercier, H. Alexander, A. Heithoff, The transcriptome and proteome of the diatom *Thalassiosira pseudonana* reveal a diverse phosphorus stress response, PLoS One 7 (3) (2012), https://doi.org/10.1371/journal.pone.0033768.
[47] H. Launay, W. Huang, S.C. Maberly, B. Gontero, Regulation of carbon metabolism by environmental conditions: a perspective from diatoms and other chromalveolates, Front. Plant Sci. 11 (July) (2020) 1–14, https://doi.org/10.3389/fpls.2020.01033.
[48] M.A. Bromke, P. Giavalisco, L. Willmitzer, H. Hesse, Metabolic analysis of adaptation to short-term changes in culture conditions of the marine diatom *Thalassiosira pseudonana*, PLoS One 8 (6) (2013) 1–11, https://doi.org/10.1371/journal.pone.0067340.
[49] Y.H. Tan, P.E. Lim, J. Beardall, S.W. Poong, S.M. Phang, A metabolomic approach to investigate effects of ocean acidification on a polar microalga *Chlorella* sp, Aquat. Toxicol. 217 (October) (2019), https://doi.org/10.1016/j.aquatox.2019.105349.
[50] L. Gauthier, J. Tison-Rosebery, S. Morin, N. Mazzella, Metabolome response to anthropogenic contamination on microalgae: a review, Metabolomics 16 (1) (2020) 1–13, https://doi.org/10.1007/s11306-019-1628-9.
[51] A.R. Fernie, R.N. Trethewey, A.J. Krotzky, L. Willmitzer, Metabolite profiling: from diagnostics to systems biology, Nat. Rev. Mol. Cell Biol. 5 (9) (2004) 763–769, https://doi.org/10.1038/nrm1451.
[52] E.V. Armbrust, J.A. Berges, C. Bowler, B.R. Green, D. Martinez, N.H. Putnam, D. S. Rokhsar, The genome of the diatom *Thalassiosira pseudonana*: ecology, evolution, and metabolism, Science 306 (5693) (2004) 79–86, https://doi.org/10.1126/science.1101156.
[53] C. Paul, M.A. Mausz, G. Pohnert, A co-culturing/metabolomics approach to investigate chemically mediated interactions of planktonic organisms reveals influence of bacteria on diatom metabolism, Metabolomics 9 (2) (2013) 349–359, https://doi.org/10.1007/s11306-012-0453-1.
[54] K.L. Poulson-Ellestad, C.M. Jones, J. Roy, M.R. Viant, F.M. Fernández, J. Kubanek, B.L. Nunn, Metabolomics and proteomics reveal impacts of chemically mediated competition on marine plankton, Proc. Natl. Acad. Sci. U. S. A. 111 (24) (2014) 9009–9014, https://doi.org/10.1073/pnas.1402130111.
[55] K. Longnecker, M.C. Kido Soule, E.B. Kujawinski, Dissolved organic matter produced by *Thalassiosira pseudonana*, Mar. Chem. 168 (2015) 114–123, https://doi.org/10.1016/j.marchem.2014.11.003.
[56] E.R. Moore, C.L. Davie-Martin, S.J. Giovannoni, K.H. Halsey, Pelagibacter metabolism of diatom-derived volatile organic compounds imposes an energetic tax on photosynthetic carbon fixation, Environ. Microbiol. 22 (5) (2020) 1720–1733, https://doi.org/10.1111/1462-2920.14861.
[57] M.A. Bromke, J.S. Sabir, F.A. Alfassi, N.H. Hajarah, S.A. Kabli, A.L. Al-Malki, L. Willmitzer, Metabolomic profiling of 13 diatom cultures and their adaptation to nitrate-limited growth conditions, PLoS One 10 (10) (2015) 1–18, https://doi.org/10.1371/journal.pone.0138965.
[58] E.B. Kujawinski, K. Longnecker, H. Alexander, S.T. Dyhrman, C.L. Fiore, S. T. Haley, W.M. Johnson, Phosphorus availability regulates intracellular nucleotides in marine eukaryotic phytoplankton, Limnol. Oceanogr. Lett. 2 (4) (2017) 119–129.
[59] K.R. Heal, N.A. Kellogg, L.T. Carlson, R.M. Lionheart, A.E. Ingalls, Metabolic consequences of cobalamin scarcity in the diatom *Thalassiosira pseudonana* as revealed through metabolomics, Protist 170 (3) (2019) 328–348, https://doi.org/10.1016/j.protis.2019.05.004.
[60] K.E. Lohr, E.F. Camp, U. Kuzhiumparambil, A. Lutz, W. Leggat, J.T. Patterson, D. J. Suggett, Resolving coral photoacclimation dynamics through coupled photophysiological and metabolomic profiling, J. Exp. Biol. 222 (8) (2019), https://doi.org/10.1242/jeb.195982.
[61] R. Cavill, D. Jennen, J. Kleinjans, J.J. Briedé, Transcriptomic and metabolomic data integration, Brief. Bioinform. 17 (5) (2016) 891–901, https://doi.org/10.1093/bib/bbv090.
[62] R.L. Guillard, Culture of phytoplankton for feeding marine invertebrates, in: Culture of Marine Invertebrate Animals, 1975, pp. 29–60.
[63] E.A. Laws, T.T. Bannister, Nutrient- and light-limited growth of *Thalassiosira fluviatilis* in continuous culture, with implications for phytoplankton growth in the ocean, Limnol. Oceanogr. 25 (3) (1980) 457–473, https://doi.org/10.4319/lo.2004.49.6.2316.
[64] R.A. Andersen (Ed.), Algal Culturing Techniques, Elsevier, 2005.
[65] S. Andrews, FastQC: A Quality Control Tool for High Throughput Sequence Data, 2010.
[66] N.A. Joshi, J.N. Fass, Sickle: A Sliding-window, Adaptive, Quality-based Trimming tool for FastQ files (Version 1.33) [Software], 2011.
[67] M.D. MacManes, On the optimal trimming of high-throughput mRNA sequence data, Front. Genet. 5 (Jan) (2014) 1–7, https://doi.org/10.3389/fgene.2014.00013.
[68] C.R. Williams, A. Baccarella, J.Z. Parrish, C.C. Kim, Trimming of sequence reads alters RNA-Seq gene expression estimates, BMC Bioinform. 17 (1) (2016) 1–13, https://doi.org/10.1186/s12859-016-0956-2.
[69] D. Kim, B. Langmead, S.L. Salzberg, HISAT: A fast spliced aligner with low memory requirements, Nat. Methods 12 (4) (2015) 357–360, https://doi.org/10.1038/nmeth.3317.
[70] M. Pertea, D. Kim, G.M. Pertea, J.T. Leek, S.L. Salzberg, Transcript-level expression analysis of RNA-seq experiments with HISAT, StringTie and Ballgown, Nat. Protoc. 11 (9) (2016) 1650–1667, https://doi.org/10.1038/nprot.2016.095.
[71] H. Li, B. Handsaker, A. Wysoker, T. Fennell, J. Ruan, N. Homer, R. Durbin, The sequence alignment/map format and SAMtools, Bioinformatics 25 (16) (2009) 2078–2079, https://doi.org/10.1093/bioinformatics/btp352.
[72] A.R. Quinlan, I.M. Hall, BEDTools: a flexible suite of utilities for comparing genomic features, Bioinformatics 26 (6) (2010) 841–842, https://doi.org/10.1093/bioinformatics/btq033.
[73] M. Pertea, G.M. Pertea, C.M. Antonescu, T.C. Chang, J.T. Mendell, S.L. Salzberg, StringTie enables improved reconstruction of a transcriptome from RNA-seq reads, Nat. Biotechnol. 33 (3) (2015) 290–295, https://doi.org/10.1038/nbt.3122.
[74] M.I. Love, S. Anders, W. Huber, Differential analysis of count data - the DESeq2 package, in: Genome Biology vol. 15, 2014. Retrieved from, http://biorxiv.org/lookup/doi/10.1101/002832%5Cnhttps://doi.org/10.1186/s13059-014-0550-8. Retrieved from.
[75] S. Anders, W. Huber, A. Dobin, C.A. Davis, F. Schlesinger, J. Drenkow, S. Bakhshi, Differential expression analysis for sequence count data via mixtures of negative binomials, Adv. Environ. Biol. 7 (10) (2010) 2803–2809.
[76] D. Tenenbaum, KEGGREST: Client-side REST Access to KEGG. R Package Version vol. 1(1), 2016.
[77] W. Luo, G. Pant, Y.K. Bhavnasi, S.G. Blanchard, C. Brouwer, Pathview web: user friendly pathway visualization and data integration, Nucleic Acids Res. 45 (W1) (2017) W501–W508, https://doi.org/10.1093/nar/gkx372.
[78] D.J. Suggett, H.L. Macintyre, R.J. Geider, Evaluation of biophysical and optical determinations of light absorption by photosystem II in phytoplankton, Limnol. Oceanogr. Methods 2 (10) (2004) 316–332, https://doi.org/10.4319/lom.2004.2.316.

[79] C.E. Sheehan, K.G. Baker, D.A. Nielsen, K. Petrou, Temperatures above thermal optimum reduce cell growth and silica production while increasing cell volume and protein content in the diatom *Thalassiosira pseudonana*, Hydrobiologia 847 (20) (2020) 4233–4248, https://doi.org/10.1007/s10750-020-04408-6.
[80] D.J. Suggett, S. Goyen, D.T. Pettay, M. Szabó, M.E. Warner, C. Evenhuis, P. J. Ralph, Functional diversity of photobiological traits within the genus Symbiodinium appears to be governed by the interaction of cell size with cladal designation, New Phytol. 208 (2) (2015) 370–381, https://doi.org/10.1111/nph.13483.
[81] Z.S. Kolber, O. Prasil, P.G. Falkowski, Measurements of variable chlorophyll fluorescence using fast repetition rate techniques: defining methodology and experimental protocols, Biochim. Biophys. Acta Bioenerg. 1367 (1998) 88–106 (Retrieved from papers2://publication/uuid/C591C675-7666-49B5-AB3C-16E2C3FCFD57).
[82] R.J. Ritchie, Consistent sets of spectrophotometric chlorophyll equations for acetone, methanol and ethanol solvents, Photosynth. Res. 89 (1) (2006) 27–41, https://doi.org/10.1007/s11120-006-9065-9.
[83] J.B. Raina, B.S. Lambert, D.H. Parks, C. Rinke, N. Siboni, M. Ostrowski, J. R. Seymour, Chemotaxis shapes the microscale organization of the ocean's microbiome, Nature (2022), https://doi.org/10.1038/s41586-022-04614-3.
[84] E.M. Sogin, E. Puskas, N. Dubilier, M. Liebeke, Marine metabolomics: a method for non-targeted measurement of metabolites in seawater by gas chromatography mass spectrometry, MSystems 4 (6) (2019) 1–14, https://doi.org/10.1101/528307.
[85] A.M. De Livera, D.A. Dias, D. De Souza, T. Rupasinghe, J. Pyke, D. Tull, T. P. Speed, Normalizing and integrating metabolomics data, Anal. Chem. 84 (24) (2012) 10768–10776, https://doi.org/10.1021/ac302748b.
[86] J. Chong, D.S. Wishart, J. Xia, Using metaboanalyst 4.0 for comprehensive and integrative metabolomics data analysis, Curr. Protoc. Bioinformatics 68 (2019), https://doi.org/10.1002/cpbi.86 e68.
[87] V.G. Tusher, R. Tibshirani, G. Chu, Significance analysis of microarrays applied to the ionizing radiation response, Proc. Natl. Acad. Sci. U. S. A. 98 (9) (2001) 5116–5121, https://doi.org/10.1073/pnas.091062498.
[88] J. Xia, N. Psychogios, N. Young, D.S. Wishart, MetaboAnalyst: a web server for metabolomic data analysis and interpretation, Nucleic Acids Res. 37 (Suppl. 2) (2009) 652–660, https://doi.org/10.1093/nar/gkp356.
[89] B.H. Junker, C. Klukas, F. Schreiber, VANTED: a system for advanced data analysis and visualization in the context of biological networks, BMC Bioinform. 7 (109) (2006) 1–13, https://doi.org/10.1186/1471-2105-7-109.
[90] M. Kanehisa, S. Goto, KEGG: Kyoto encyclopedia of genes and genomes, Nucleic Acids Res. 28 (1) (2000) 27–30.
[91] V.S. Stonik, I. Stonik, Low-molecular-weight metabolites from diatoms: structures, biological roles and biosynthesis, Mar. Drugs 13 (6) (2015) 3672–3709, https://doi.org/10.3390/md13063672.
[92] H.P. Dong, Y.L. Dong, L. Cui, S. Balamurugan, J. Gao, S.H. Lu, T. Jiang, High light stress triggers distinct proteomic responses in the marine diatom *Thalassiosira pseudonana*, BMC Genomics 17 (1) (2016) 1–14, https://doi.org/10.1186/s12864-016-3335-5.
[93] W.B. Penta, J. Fox, K.H. Halsey, Rapid photoacclimation during episodic deep mixing augments the biological carbon pump, Limnol. Oceanogr. 66 (5) (2021) 1850–1866, https://doi.org/10.1002/lno.11728.
[94] M.J. Behrenfeld, K.H. Halsey, E. Boss, L. Karp-Boss, A.J. Milligan, G. Peers, Thoughts on the evolution and ecological niche of diatoms, Ecol. Monogr. 91 (3) (2021) 1–25, https://doi.org/10.1002/ecm.1457.
[95] A. Gruber, P.G. Kroth, Intracellular metabolic pathway distribution in diatoms and tools for genome-enabled experimental diatom research, Philos. Trans. Royal Soc. B: Biol. Sci. 372 (1728) (2017), https://doi.org/10.1098/rstb.2016.0402.
[96] S.R. Smith, R.M. Abbriano, M. Hildebrand, Comparative analysis of diatom genomes reveals substantial differences in the organization of carbon partitioning pathways, Algal Res. 1 (1) (2012) 2–16.
[97] G. Michel, T. Tonon, D. Scornet, J.M. Cock, B. Kloareg, Central and storage carbon metabolism of the brown alga *Ectocarpus siliculosus*: insights into the origin and evolution of storage carbohydrates in Eukaryotes, New Phytol. 188 (1) (2010) 67–81, https://doi.org/10.1111/j.1469-8137.2010.03345.x.
[98] T. Obata, S. Schoenefeld, I. Krahnert, S. Bergmann, A. Scheffel, A.R. Fernie, Gas-chromatography mass-spectrometry (GC-MS) based metabolite profiling reveals mannitol as a major storage carbohydrate in the coccolithophorid Alga Emiliania huxleyi, Metabolites 3 (1) (2013) 168–184, https://doi.org/10.3390/metabo3010168.
[99] V. Villanova, A.E. Fortunato, D. Singh, D.D. Bo, M. Conte, T. Obata, G. Finazzi, Investigating mixotrophic metabolism in the model diatom *Phaeodactylum tricornutum*, Philos. Trans. Royal Soc. B: Biol. Sci. 372 (1728) (2017), https://doi.org/10.1098/rstb.2016.0404.
[100] K. Roberts, E. Granum, R.C. Leegood, J.A. Raven, Carbon acquisition by diatoms, Photosynth. Res. 93 (1–3) (2007) 79–88, https://doi.org/10.1007/s11120-007-9172-2.
[101] M. Fabris, M. Matthijs, S. Carbonelle, T. Moses, J. Pollier, R. Dasseville, A. Goossens, Tracking the sterol biosynthesis pathway of the diatom *Phaeodactylum tricornutum*, New Phytol. 204 (3) (2014) 521–535, https://doi.org/10.1111/nph.12917.
[102] J.P. Sachs, O.E. Kawka, The influence of growth rate on 2H/1H fractionation in continuous cultures of the coccolithophorid *Emiliania huxleyi* and the diatom *Thalassiosira pseudonana*, PLoS One 10 (11) (2015) 1–27, https://doi.org/10.1371/journal.pone.0141643.
[103] A.C. Jaramillo-Madrid, J. Ashworth, M. Fabris, P.J. Ralph, The unique sterol biosynthesis pathway of three model diatoms consists of a conserved core and diversified endpoints, Algal Res. 48 (October 2019) (2020) 101902, https://doi.org/10.1016/j.algal.2020.101902.
[104] S.C. Bhatla, M.A. Lal, Chp. 7: Respiration, in: Plant Physiology, Development and Metabolism, 2018.
[105] Q. Lin, J.R. Liang, Q.Q. Huang, C.S. Luo, D.M. Anderson, C. Bowler, Y.H. Gao, Differential cellular responses associated with oxidative stress and cell fate decision under nitrate and phosphate limitations in *Thalassiosira pseudonana*: comparative proteomics, PLoS One 12 (9) (2017) 1–27, https://doi.org/10.1371/journal.pone.0184849.
[106] U. Winkler, H. Stabenau, Isolation and characterization of peroxisomes from diatoms, Planta 195 (3) (1995) 403–407.
[107] M. Kunze, I. Pracharoenwattana, S.M. Smith, A. Hartig, A central role for the peroxisomal membrane in glyoxylate cycle function, Biochim. Biophys. Acta (BBA)-Mol. Cell Res. 1763 (12) (2006) 1441–1452.
[108] N.H. Gonzalez, G. Felsner, F.D. Schramm, A. Klingl, U.G. Maier, K. Bolte, A single peroxisomal targeting signal mediates matrix protein import in diatoms, PLoS One 6 (9) (2011), e25316.
[109] L.L. Cross, H.T. Ebeed, A. Baker, Peroxisome biogenesis, protein targeting mechanisms and PEX gene functions in plants, Biochim. Biophys. Acta, Mol. Cell Res. 1863 (5) (2016) 850–862, https://doi.org/10.1016/j.bbamcr.2015.09.027.
[110] M. Giordano, M. Palmucci, J.A. Raven, Growth rate hypothesis and efficiency of protein synthesis under different sulphate concentrations in two green algae, Plant Cell Environ. 38 (11) (2015) 2313–2317, https://doi.org/10.1111/pce.12551.
[111] M. Jahn, V. Vialas, J. Karlsen, G. Maddalo, F. Edfors, B. Forsström, E.P. Hudson, Growth of cyanobacteria is constrained by the abundance of light and carbon assimilation proteins, Cell Rep. 25 (2) (2018) 478–486 (e8), https://doi.org/10.1016/j.celrep.2018.09.040 (e8).
[112] J. Beardall, Photosynthesis and photorespiration in marine organisms: photosynthesis and photorespiration in marine phytoplankton, Aquat. Bot. 34 (1989) 105–130.
[113] M.S. Parker, E.V. Armbrust, Synergistic effects of light, temperature, and nitrogen source on transcription of genes for carbon and nitrogen metabolism in the centric diatom *Thalassiosira pseudonana* (Bacillariophyceae), J. Phycol. 41 (6) (2005) 1142–1153, https://doi.org/10.1111/j.1529-8817.2005.00139.x.
[114] D. Shi, W. Li, B.M. Hopkinson, H. Hong, D. Li, S.J. Kao, W. Lin, Interactive effects of light, nitrogen source, and carbon dioxide on energy metabolism in the diatom *Thalassiosira pseudonana*, Limnol. Oceanogr. 60 (5) (2015) 1805–1822, https://doi.org/10.1002/lno.10134.